MicroRNA-709 Mediates Acute Tubular Injury through Effects on Mitochondrial Function

Yan Guo,*† Jiajia Ni,* Shuang Chen,*† Mi Bai,*†‡ Jiajuan Lin,* Guixia Ding,*† Yue Zhang,*† Pingping Sun,§ Zhanjun Jia,*†‡ Songming Huang,*† Li Yang,§ and Aihua Zhang*†‡

*Department of Nephrology, State Key Laboratory of Reproductive Medicine, Children's Hospital of Nanjing Medical University, Nanjing, China; †Jiangsu Key Laboratory of Pediatrics, Nanjing Medical University, Nanjing, China; ‡Nanjing Key Laboratory of Pediatrics, Children's Hospital of Nanjing Medical University, Nanjing, China; and §Renal Division, Peking University First Hospital, Beijing, China

ABSTRACT

Mitochondrial dysfunction has important roles in the pathogenesis of AKI, yet therapeutic approaches to improve mitochondrial function remain limited. In this study, we investigated the pathogenic role of microRNA-709 (miR-709) in mediating mitochondrial impairment and tubular cell death in AKI. In a cisplatin-induced AKI mouse model and in biopsy samples of human AKI kidney tissue, miR-709 was significantly upregulated in the proximal tubular cells (PTCs). The expression of miR-709 in the renal PTCs of patients with AKI correlated with the severity of kidney injury. In cultured mouse PTCs, overexpression of miR-709 markedly induced mitochondrial dysfunction and cell apoptosis, and inhibition of miR-709 ameliorated cisplatin-induced mitochondrial dysfunction and cell injury. Further analyses showed that mitochondrial transcriptional factor A (TFAM) is a target gene of miR-709, and genetic restoration of TFAM attenuated mitochondrial dysfunction and cell injury induced by cisplatin or miR-709 overexpression *in vitro*. Moreover, antagonizing miR-709 with an miR-709 antagomir dramatically attenuated cisplatin-induced kidney injury and mitochondrial dysfunction in mice. Collectively, our results suggest that miR-709 has an important role in mediating cisplatin-induced AKI *via* negative regulation of TFAM and subsequent mitochondrial dysfunction. These findings reveal a pathogenic role of miR-709 in acute tubular injury and suggest a novel target for the treatment of AKI.

J Am Soc Nephrol 29: ●●●–●●●, 2017. doi: https://doi.org/10.1681/ASN.2017040381

AKI has become a worldwide public health problem associated with increased morbidity and mortality.[1,2] AKI has been estimated to affect more than 13.3 million patients and results in approximately 1.7 million deaths worldwide each year.[3] Currently, no therapies are available to treat established AKI, which greatly limits clinical efforts to improve the outcomes of the patient and the patient's kidney.[4,5] Renal tubular cells are densely packed with mitochondria, which play a dual role as the primary source of energy for each cell and the key regulator of cell death.[6] Mitochondrial dysfunction is currently thought to be central to the pathogenesis of AKI by increasing reactive oxygen species (ROS) production, decreasing membrane potential, and releasing proapoptotic factors, ultimately leading to renal tubular cell death.[7–10] Therefore, mitochondria could act as potential targets for novel therapeutic intervention to alleviate tubular injury and hasten tissue recovery in AKI.

MicroRNAs (miRNAs) are small, endogenous, noncoding RNA molecules of 21–25 nucleotides

Received April 5, 2017. Accepted September 20, 2017.

Published online ahead of print. Publication date available at www.jasn.org.

Correspondence: Prof. Aihua Zhang, Department of Nephrology, State Key Laboratory of Reproductive Medicine, Children's Hospital of Nanjing Medical University, 72 Guangzhou Road, Nanjing 210029, Jiangsu Province, China, or Prof. Li Yang, Renal Division, Peking University First Hospital, Peking University, 8 Xishiku St, Xicheng District, Beijing 100034, China. E-mail: zhaihua@njmu.edu.cn or li.yang@bjmu.edu.cn

that have roles in diverse pathologic processes, such as oxidative stress, tissue injury, and metabolic disorders.[11,12] miRNAs normally bind to the 3′-untranslated region (UTR) of target mRNA transcripts, resulting in translational silencing, translation inhibition, and/or mRNA degradation.[13–15] Recently, miRNAs, including miR-15b, miR-16, miR-195, and miR-424, have been found to modulate mitochondrial function in neurons and cancer cells[16–18] by targeting ADP-ribosylation factor-like 2 mRNA or mitochondrial OXPHOS, thereby regulating ATP production. In the kidney, miR-335 and miR-34a were reported to be regulators of mesangial cell senescence by targeting the mitochondria-localized genes SOD2 and thioredoxin reductase 2,[19] and miR-30e was shown to play a profibrotic role by targeting mitochondrial uncoupling protein 2.[20] However, knowledge of the potential roles of miRNAs in modulating mitochondrial function during the process of AKI is very limited.

Previously, we conducted a high-throughput microarray assay to screen miRNA expression in the kidneys of mice with cisplatin-induced AKI. Among the miRNAs that were identified, miR-709 was shown to be consistently enhanced *in vitro* and *in vivo*. To date, the role of miR-709 has not been well defined. Recently, several studies have shown that miR-709 is involved in 3T3-L1 cell differentiation, hepatocellular carcinoma development, and inflammatory response in macrophages.[21–23] However, there have not been any reports demonstrating the involvement of miR-709 in kidney diseases. Herein, by using an animal model, *in vitro* proximal tubular cells (PTCs), and human renal biopsy samples, we are the first to demonstrate that miR-709 is upregulated and plays an important role in mediating cisplatin nephrotoxicity by inducing mitochondrial dysfunction. These findings suggest a pathogenic role of miR-709 in acute tubular injury and offer a novel target for treating AKI.

RESULTS

Confirmation of miR-709 Upregulation in Renal Tubular Cells Exposed to Cisplatin Nephrotoxicity and in Human AKI

We first confirmed upregulation of miR-709 in the kidney cortex of the cisplatin-induced AKI mouse model 3 days after cisplatin injection (Figure 1A). Through *in situ* hybridization, upregulation of miR-709 was detected primarily in the renal tubular cells (Figure 1B). Next, in cultured mouse proximal tubular epithelial cells (mPTCs), treatment with cisplatin induced significant overexpression of miR-709 in both a dose- and time-dependent manner (Figure 1, C and D).

To explore the association between miR-709 and human AKI, we performed *in situ* hybridization of miR-709 with a Cy3-labeled probe (RiboBio, Guangzhou, China) in biopsied kidney tissue from 21 patients with various forms of AKI resulting from ischemic, nephrotoxic, or combined insults. Para-carcinoma kidney tissue from seven patients who underwent renal carcinoma resection were used as controls. The clinical features of the patients with AKI are listed in Table 1.

Significance Statement

Mitochondrial dysfunction plays an important role in the pathogenesis of acute kidney injury (AKI), but therapeutic approaches to improve mitochondrial function are still limited. microRNAs are receiving increased attention as possible targets for therapy of AKI. In the present study, in both the cisplatin-induced AKI mouse model and human AKI kidney biopsies, miR-709 was found to be upregulated in the proximal tubular cells (PTCs); expression of miR-709 was correlated with severity of kidney injury. Furthermore, inhibition of miR-709 ameliorated cisplatin-induced mitochondrial dysfunction and cell injury. Further analyses showed that TFAM (mitochondrial transcription factor A) is a target gene of miR-709. The results support a detrimental role of miR-709 in mediating cisplatin-induced AKI possibly via targeting mitochondrial gene TFAM and subsequent mitochondrial dysfunction.

As shown in Figure 1, E–H and consistent with the observations in the cisplatin-induced mouse AKI, significant overexpression of miR-709 was detected, predominantly in aquaporin 1–positive renal tubular cells in the kidney tissue of patients with AKI compared with the control kidney tissue samples. Further analysis showed that the degree of miR-709 overexpression in renal tubular cells was correlated with the severity of tubular damage (r=0.52, P=0.02) (Figure 1I) and the peak levels of serum creatinine (r=0.44, P=0.049) (Figure 1J), indicating an association between miR-709 and the pathogenesis of renal tubular injury.

Overexpression of miR-709 Contributes to Mitochondrial Dysfunction and Cell Death in mPTCs

To understand the potential pathophysiological role of miR-709 upregulation in renal tubular cells, we first transfected an miR-709 mimic into mPTCs (Figure 2A). As shown in Figure 2, B–G, there was notable mitochondrial dysfunction in the miR-709–transfected mPTCs compared with the cells transfected with the negative control, as determined by the reductions in the mitochondrial membrane potential level ($\Delta\psi$m), oxygen consumption rate (OCR), mitochondrial DNA (mtDNA) copy number, and mitochondrial protein CytB expression, along with an increase in mitochondrial superoxide (mitoSOX) production. In parallel with the mitochondrial dysfunction, significantly enhanced apoptosis was observed in the miR-709 mimic-transfected mPTCs compared with the mPTCs transfected with the negative control, as reflected by the flow cytometry assay of annexin-V–stained cells and the activity analysis of caspase-3 (Figure 2, H and I). These findings indicate that overexpression of miR-709 in PTCs can induce mitochondrial dysfunction and cell death.

miR-709 Targets Mitochondrial Transcriptional Factor A To Induce Tubular Mitochondrial Dysfunction and Cell Death

To study the molecular mechanism of miR-709 in modulating mitochondrial function, we performed a bioinformatics analysis (using TargetScan, PicTar Genome, and RNA Hybrid) to identify its potential targets and found evolutionarily conserved binding sites for miR-709 in the 3′-UTR of

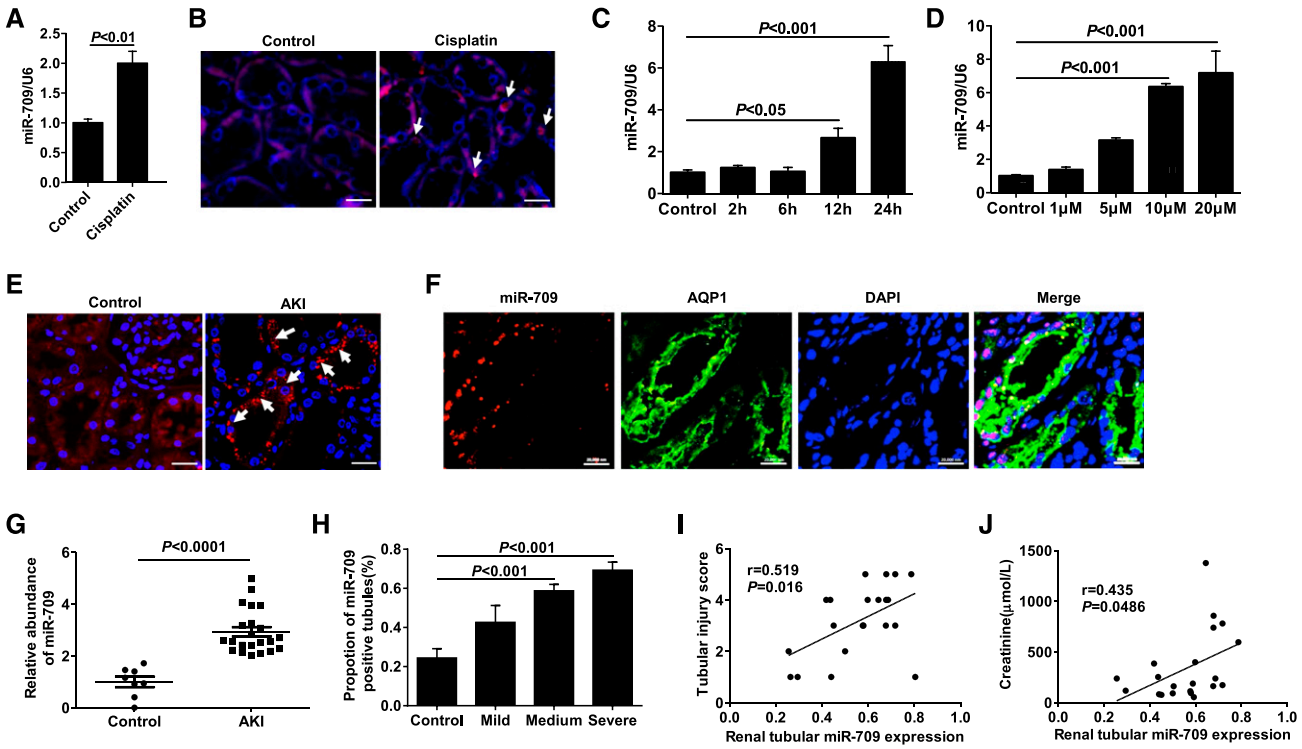

Figure 1. miR-709 is upregulated in murine renal tubular cells exposed to cisplatin insult and in patients with AKI. (A and B) Quantitative real-time PCR (qPCR) analysis (A) and fluorescence *in situ* hybridization (B) of miR-709 in a cisplatin-induced AKI mouse model (on day 3 after cisplatin injection); *n*= 6 animals per group. White arrows indicate the location of increased miR-709 expression in renal tubular cells. C57BL/6 mice were injected intraperitoneally with cisplatin at 20 mg/kg body wt. (C and D) qPCR analysis of miR-709 in the mPTCs treated with cisplatin for various times (10 μM for 0–24 hours) and at various dosages (0–20 μM for 24 hours). (E) Fluorescence *in situ* hybridization of miR-709 in kidney tissue biopsy samples from patients with AKI (*n*=21) and para-carcinoma kidney tissue (*n*=7). White arrows indicate the location of increased miR-709 expression in renal tubular cells. (F) Colocalization of miR-709 with aquaporin 1 (AQP1) in kidney biopsy tissue from patients with AKI. AQP1 was used as a marker for proximal tubules. Biopsied kidney tissue from patients with AKI were triple-labeled with miR-709 (red, Cy3), AQP1 (green, FITC), and 4′,6-diamidino-2-phenylindole (blue). Scale bar, 20 μm. (G) Quantification of miR-709 in kidney tissue biopsy samples. (H and I) The correlation between renal tubular expression of miR-709 and the severity of tubular injury in patients with AKI. (J) The correlation between renal tubular expression of miR-709 and the peak level of serum creatinine in patients with AKI. Data are expressed as mean±SEM. Scale bar, 50 μm. For each experiment, differences between means were considered statistically significant at $P<0.05$.

mitochondrial transcriptional factor A (TFAM). TFAM plays a key role in the biosynthesis of mtDNA and mitochondrial function maintenance[24]; thus, we hypothesized that miR-709 can directly target TFAM in mPTCs. To test this hypothesis, we transfected pcDNA-TFAM and miR-709 mimic into the mPTCs (Figure 3, A and B). As shown in Figure 3, A and B, the miR-709 mimic significantly reduced TFAM expression at both the mRNA and protein levels. To determine whether TFAM is a direct target of miR-709, the normal sequence of the TFAM 3′-UTR (wild-type) or a mutant sequence with three nucleotides changed in the region corresponding to the miR-709 "seed" sequence was fused into a luciferase reporter plasmid and transiently transfected into the mPTCs, along with an miR-709 mimic or a negative control. As shown in Figure 3C, cotransfection of miR-709 significantly decreased the luciferase activity of the wild-type TFAM 3′-UTR but not the mutant TFAM 3′-UTR, demonstrating that miR-709 directly inhibits the transcription of the *TFAM* gene in mPTCs.

To test whether the inhibition of TFAM mediates the detrimental effects of miR-709 on tubular mitochondrial function and cell survival, we cotransfected mPTCs with miR-709 mimic

Table 1. Demographic and clinical data of patients with AKI

Characteristic	Patients with AKI
N	21
Men, *n* (%)	11 (52)
Age, yr	49.0±12.7
Causes of AKI, *n* (%)	
Nephrotoxins[a]	12 (57)
Ischemia	1 (5)
Combined	8 (38)
Serum creatinine at peak, μmol/L	227.7 (116.3 to 728.5)
Serum creatinine at biopsy, μmol/L	188.0 (103.8 to 392.5)

Data for age are mean±SD and for serum creatinine are median (interquartile range). Normal range for serum creatinine: 40–133 μmol/L.
[a]Nephrotoxins included antimicrobial agents in nine patients, acetaminophen in one patient, herbal medicine in one patient, and monoclonal gammopathy in one patient.

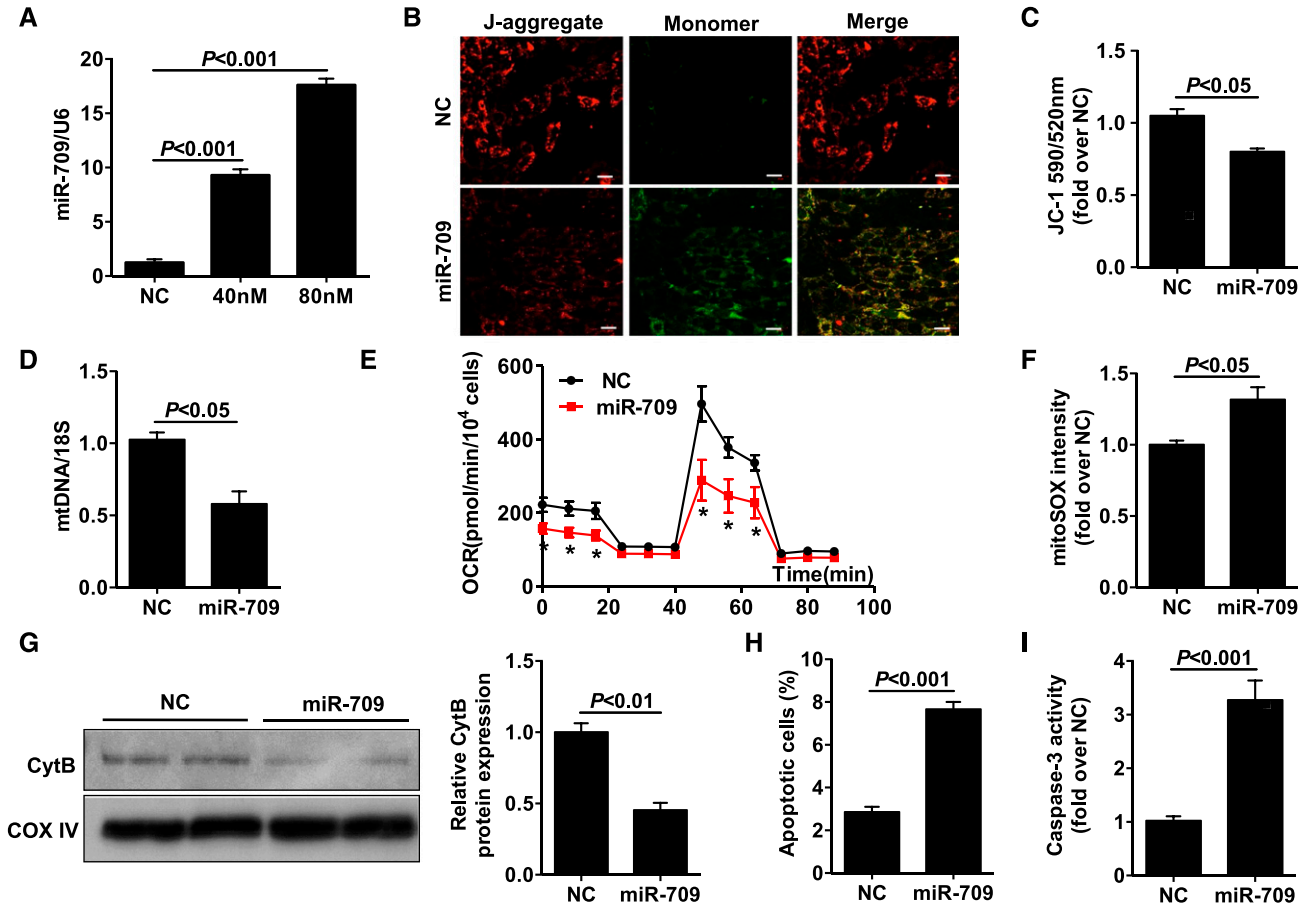

Figure 2. Overexpression of miR-709 contributes to mitochondrial dysfunction and cell death in mPTCs. (A) Quantitative real-time PCR (qPCR) analysis of miR-709 expression in mPTCs. mPTCs were transfected with miR-709 mimic (40 or 80 nM) for 24 hours. (B) Representative confocal microscopy images of JC-1 staining; red fluorescence represents the mitochondrial aggregate JC-1 and green fluorescence indicates the monomer JC-1. Scale bar, 20 μm. (C) Quantification of JC-1 fluorescence *via* flow cytometry. (D) qPCR analysis of mtDNA copy number. (E) OCR. (F) Quantification of the mitoSOX signal using flow cytometry. (G) Western blotting analysis of CytB. mPTCs were transfected with miR-709 mimic (80 nM) or negative control (NC, 40 nM) for 24 hours. (H) Flow cytometry assay of annexin V–stained cells. (I) Caspase-3 activity. mPTCs were transfected with miR-709 mimic (80 nM) or NC (40 nM) for 48 hours. Values are presented as mean±SEM (n= 4–8 per group). For each experiment, differences between means were considered statistically significant when $P<0.05$.

and pcDNA-TFAM. As shown in Figure 3, D–H, the decrements in $\Delta\psi$m, OCR, and mtDNA copy number, and the increase in mitochondrial ROS induced by miR-709 mimic transfection were significantly alleviated by TFAM overexpression. Further, the increased cell apoptosis induced by miR-709 overexpression was also attenuated by genetic restoration of TFAM in parallel with inhibition of caspase-3 activity (Figure 3, I and J). These results demonstrate that upregulation of miR-709 mediates renal PTC injury by negatively regulating the nuclear gene *TFAM* and subsequently altering mitochondrial function.

Targeting miR-709 and TFAM Attenuates Mitochondrial Dysfunction and Cell Death in Cultured mPTCs Exposed to Cisplatin

Because miR-709 has been found to be upregulated dramatically in cisplatin-induced mouse AKI, and activation of the miR-709/TFAM axis has been confirmed to mediate tubular mitochondrial dysfunction and cell apoptosis, we performed further experiments to assess whether targeting miR-709 and TFAM could alleviate cisplatin-induced tubular cell injury. We first confirmed the response of the miR-709/TFAM axis in cultured PTCs after cisplatin challenge. As shown in Figure 4, A–D, TFAM was inhibited in mPTCs after cisplatin treatment in a dose- and time-dependent manner at both the mRNA and protein level, which was concomitant with the upregulation of miR-709. Moreover, depletion of TFAM significantly reduced cell viability and increased apoptosis in mPTCs (Figure 4, E and F).

We then inhibited miR-709 by transfecting the mPTCs with an anti–miR-709 inhibitor and found that the reduction in TFAM induced by cisplatin treatment was largely abolished by inhibition of miR-709 (Figure 4, G and H). Also, the mitochondrial dysfunction evidenced by reduced $\Delta\psi$m and

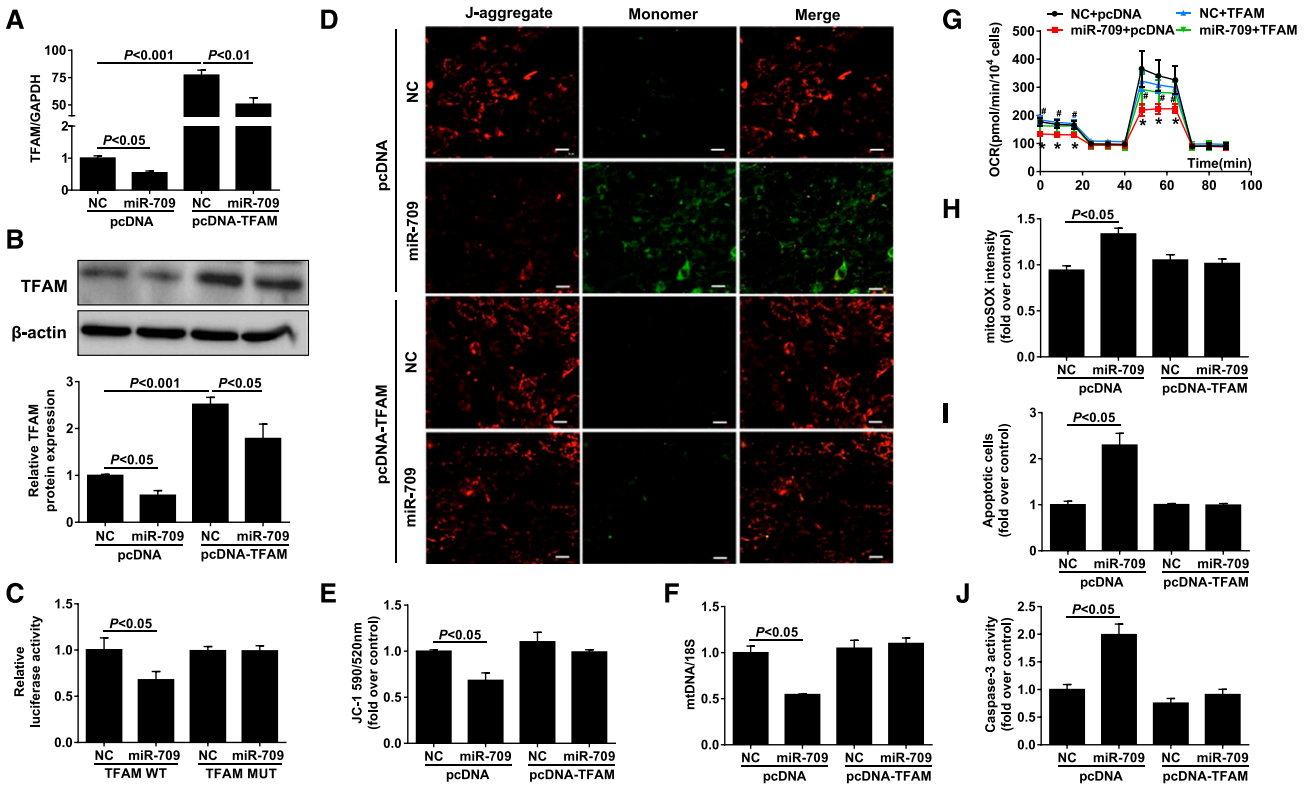

Figure 3. miR-709 induces mitochondrial dysfunction and cell death by targeting TFAM. (A) Quantitative real-time PCR (qPCR) analysis of TFAM mRNA expression in mPTCs. (B) Western blotting analysis of TFAM protein expression in mPTCs. Upper panel: representative immunoblots. Lower panel: densitometric analysis. mPTCs were cotransfected with miR-709 mimic (80 nM) and pcDNA3.1-TFAM or pcDNA3.1 empty vector for 24 hours. (C) Luciferase assays of the mPTCs cotransfected with TFAM luciferase reporter (WT) and miR-709 mimic (80 nM) or mutant TFAM luciferase reporter (MUT) for 24 hours. (D) Representative confocal microscopy images of JC-1 staining; red fluorescence represents the mitochondrial aggregate JC-1 and green fluorescence indicates the monomer JC-1. Scale bar, 20 μm. (E) Quantification of JC-1 fluorescence using flow cytometry. (F) qPCR analysis of mtDNA copy number. (G) OCR. (H) Quantification of the mitoSOX signal using flow cytometry. (I) Flow cytometry assay of annexin-V–stained cells. (J) Caspase-3 activity. mPTCs were cotransfected with miR-709 mimic (80 nM) and pcDNA3.1-TFAM for 24 hours. Values are presented as mean±SEM (n= 4–8 per group). *P<0.05, miR-709 plus pcDNA versus negative control plus pcDNA. $^{\#}P$<0.05, miR-709 plus pcDNA versus miR-709 plus TFAM. For each experiment, differences between means were considered statistically significant when P<0.05.

OCR, the decreased mtDNA copy number, and the increased mitochondrial ROS production triggered by cisplatin treatment was significantly reversed by miR-709 inhibition (Figure 5, A–E). The cellular apoptosis induced by cisplatin was also attenuated, corresponding with the blockade of caspase-3 activation (Figure 5, F and G). Next, overexpression of TFAM by transfection with pcDNA-TFAM markedly ameliorated cell apoptosis, blocked caspase-3 activation, and protected mitochondrial function in mPTCs treated with cisplatin (Figure 5, A–G). These results suggested that the miR-709/TFAM axis contributed to the cisplatin-induced mitochondrial dysfunction and mPTC apoptosis, and therefore might act as a potential therapeutic target.

miR-709 Antagomir Attenuates Kidney Injury and Mitochondrial Dysfunction in Mouse Cisplatin-Induced AKI

To further confirm the *in vivo* role of miR-709 in cisplatin-induced kidney injury, an miR-709 antagomir was administered to the mice before cisplatin injection. As shown in Figure 6A, the miR-709 antagomir substantially reduced the miR-709 level by 72% in mice kidneys after cisplatin-induced injury. Notably, the inhibition of miR-709 *in vivo* significantly reduced the degree of renal dysfunction assessed by the levels of serum creatinine and BUN, improved renal histologic damage, alleviated tubular cell apoptosis, and reduced the mortality rate of mice after cisplatin treatment (Figure 6, B–H). Moreover, inhibition of miR-709 before cisplatin injection markedly ameliorated TFAM down-regulation and protected the mitochondrial function in mice kidneys, as reflected by the reduced mitochondrial ROS production and the attenuation of decreased $\Delta\psi$m, mitochondrial complex I activity, mtDNA copy number, and mitochondrial protein CytB expression (Figure 7, A–H). These data offer *in vivo* evidence showing that miR-709 plays an important role in mediating cisplatin-induced AKI, and reinforce the potential of miR-709 as a novel therapeutic target in preventing acute tubular injury.

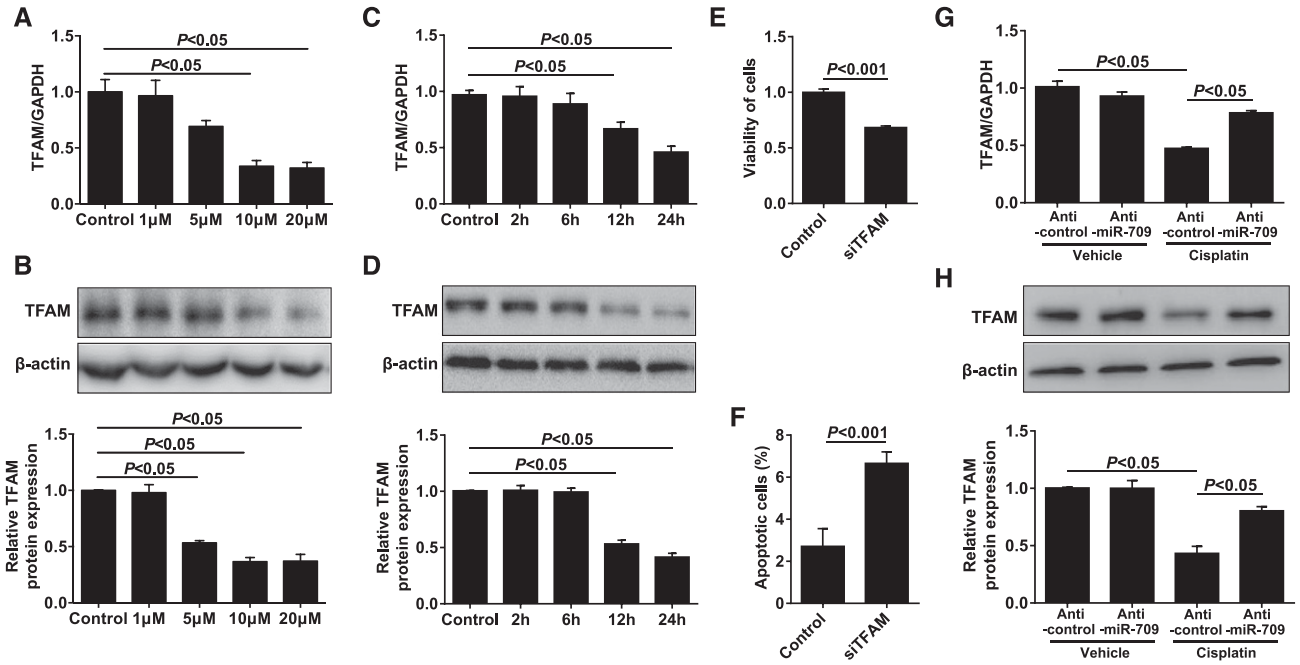

Figure 4. Antagonism of miR-709 blocks the cisplatin-induced reduction in TFAM expression. (A and C) Quantitative real-time PCR (qPCR) analysis of TFAM mRNA expression. (B and D) Western blotting analysis of TFAM protein expression. mPTCs were treated with cisplatin at various dosages (0–20 μM for 24 hours) (A and B) and for various times (10 μM for 0–24 hours) (C and D). (E) Analysis of cell viability. mPTCs were transfected with TFAM small interfering RNA (siRNA) or control siRNA for 24 hours. Cell viability was measured by Cell Counting Kit 8 assay. (F) Flow cytometry assay of annexin-V–stained cells. mPTCs were transfected with TFAM siRNA or control siRNA for 48 hours. (G) qPCR analysis of TFAM mRNA expression. (H) Western blotting analysis of TFAM protein expression. mPTCs were transfected with miR-709 mimic (80 nM) for 24 hours and then treated with cisplatin (10 μM) for an additional 24 hours. Data are presented as mean±SEM (n= 4–8 per group). For each experiment, differences between means were considered statistically significant when $P<0.05$.

DISCUSSION

Mitochondria undergo significant alterations during AKI, with functional and structural damage appearing much earlier than the clinical and pathologic manifestations of kidney injury induced by ischemic,[25,26] nephrotoxic,[27,28] and septic insults.[29–31] As the key source of cellular energy, mitochondria play critical roles in the pathophysiology of kidney injury as well as in the recovery from injury.[32,33] Therefore, a more complete molecular understanding of mitochondrial damage has become an area of exploration for the development of novel therapies for AKI. In this study, we first reported upregulation of miR-709 and its pathogenic role in mediating mitochondrial dysfunction and subsequent cell death in the renal PTCs of mouse cisplatin-induced AKI, which verifies its increased expression and potential relationship with the pathogenesis of human AKI of various etiologies. We further demonstrated the applicability of anti–miR-709 treatment in preventing cisplatin-induced AKI in mice.

miR-709 is reported to be abundantly expressed in multiple mouse tissues, such as the brain, thymus, heart, and liver.[34–37] In addition, miR-709 acts on multiple genes, including Egr2, c-Jun, Sox-2, c-Myc, Akt, Ras-GRF1, GSK3β, ET-1, and Pctp, and plays different roles in various organs, such as promoting carcinoma migration and invasiveness, inhibiting adipocyte differentiation, and inducing the macrophage inflammatory response.[21,35,38] Thus far, the knowledge of miR-709 in the kidney is limited to cultured murine inner medullary collecting duct cells, where it might affect endothelin 1 expression,[34] although its role in kidney injury remains unknown. In this study, we took advantage of a mouse cisplatin-induced AKI model and first reported a prominent upregulation of miR-709 primarily in the renal tubular cells after acute injury. Moreover, the renal tubular mitochondrial dysfunction and cell apoptosis induced by cisplatin insult was almost completely blocked by anti–miR-709 management both *in vitro* and *in vivo*, suggesting a pathogenic role of miR-709 through mitochondrial damage in this kidney toxic injury model. In kidney tissue biopsy samples from patients with clinical AKI resulting from various causes, including ischemia and different types of nephrotoxins, we confirmed the upregulation of miR-709 in human injured tubular cells and detected a significant correlation between the expression of tubular miR-709 and the severity of tissue damage, as well as the degree of renal dysfunction. Furthermore, overexpression of miR-709 alone in cultured mouse PTCs directly induced mitochondrial

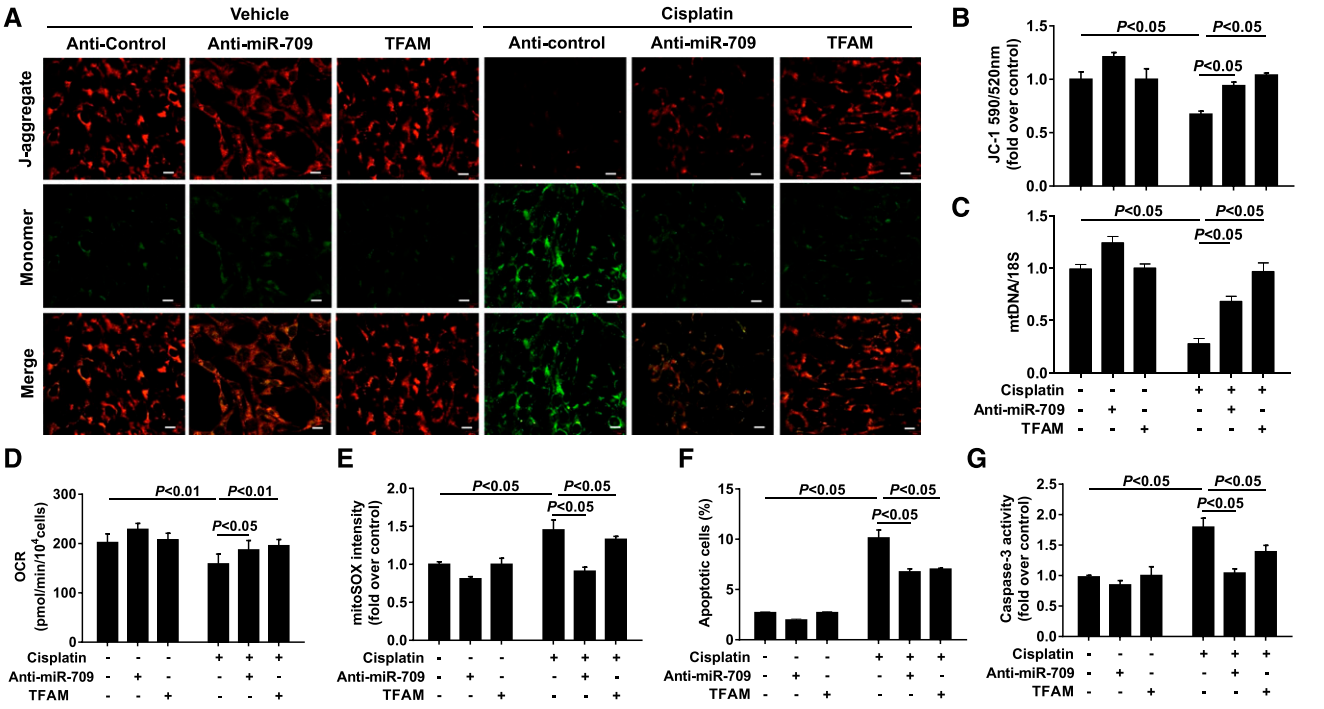

Figure 5. Targeting miR-709 and TFAM attenuates cisplatin-induced mitochondrial dysfunction and cell death in cultured mPTCs. (A) Representative confocal microscopy images of JC-1 staining; red fluorescence represents the mitochondrial aggregate JC-1 and green fluorescence indicates the monomer JC-1. Scale bar, 10 μm. (B) Quantification of JC-1 fluorescence using flow cytometry. (C) qPCR analysis of mtDNA copy number. (D) OCR. (E) Quantification of the mitoSOX signal using flow cytometry. (F) Flow cytometry assay of annexin-V–stained cells. (G) Caspase-3 activity. mPTCs were transfected with miR-709 inhibitor (80 nM) or pcDNA3.1-TFAM for 24 hours and then treated with cisplatin (10 μM) for an additional 24 hours. Values are presented as mean±SEM (n= 4–8 in each group). For each experiment, differences between means were considered statistically significant when $P<0.05$.

dysfunction and ultimately cell apoptosis. These data indicate that increased expression of miR-709 in tubular cells after acute insult could be a common mediator of mitochondrial damage and cell death, and therefore might serve as a potential therapeutic target for treating AKI.

Next, we identified TFAM, a transcriptional factor, as a specific target of miR-709 in mediating renal tubular mitochondrial dysfunction and cell apoptosis. To date, TFAM is the only known protein that fulfills the stringent definition of a structural component that packages mtDNA in the mammalian nucleoid and is an essential component of the mammalian mtDNA transcription initiation complex.[39] Therefore, TFAM is critical for the replication, transcription, maintenance, and repair of mtDNA[40–42] to preserve mitochondrial biogenesis and normal function. Lack of this transcription factor in systemic TFAM-knockout mice resulted in severe mtDNA depletion and embryonic lethality.[43] In this study, we showed that upregulation of miR-709 significantly suppressed TFAM at both the mRNA and protein levels by directly targeting its 3′-UTR sites, and overexpression of TFAM could rescue mitochondrial function as well as the tubular cell death induced through miR-709 upregulation. These results demonstrate that miR-709 targets the critical mitochondrial protective protein TFAM and impairs the biogenesis of the mitochondria in the renal tubular cells after acute insult.

Although the important role of mitochondrial impairment in the process of acute tissue injury has been widely acknowledged, intervention to improve mitochondrial function remains a huge pharmacologic challenge because of the difficulty of developing medications that can specifically target and access these organelles.[44] Our study provides the possibility of protecting mitochondria from injury through modulation of a mitochondrial functional protein by targeting its upstream miRNA. We administered an miR-709 antagonist to the mice before cisplatin treatment and established significant protection against tubular mitochondrial dysfunction, as evidenced by the decrease in mitochondrial ROS production and the restoration of mtDNA copy number, mitochondrial protein CytB expression, complex I activity, and $\Delta\psi$m. The degree of renal dysfunction, tubular cell necrosis and apoptosis, and the mortality rate of mice were also ameliorated by anti–miR-709 oligonucleotides. Recently, advances in oligonucleotide chemistry have allowed for the development of engineered oligonucleotides directed against specific miRNAs, which can be taken up freely into cells and specifically block the function of certain miRNAs.[45] As an example, RG-012, a single-stranded, chemically modified oligonucleotide that can bind and inhibit the function of miR-21, has been developed as a potent inhibitor of miR-21 and could effectively ameliorate kidney fibrosis in rodent models of Alport syndrome.[45]

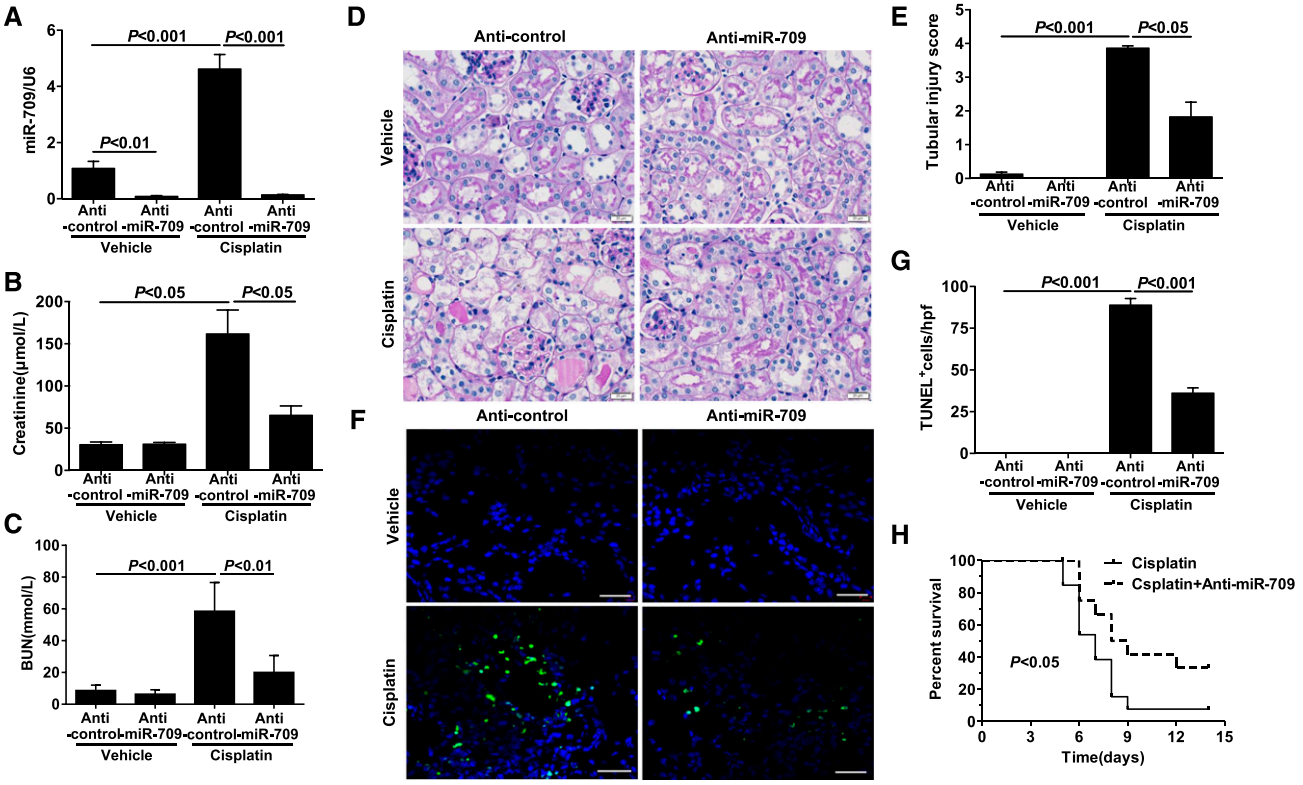

Figure 6. miR-709 antagomir attenuates kidney injury in mouse cisplatin-induced AKI. (A) Quantitative real-time PCR (qPCR) analysis of miR-709 expression in the kidney cortex. (B) Serum creatinine. (C) BUN. (D) Representative images of renal PAS staining. Scale bar, 20 μm. (E) Tubular injury score. (F) Representative images of TUNEL staining. Scale bar, 50 μm. (G) Quantification of TUNEL-positive cells in the kidney. C57BL/6 mice were treated with miR-709 antagomir (anti–miR-709, 20 mg/kg, intraperitoneal [i.p.]) or anti-control for 24 hours and then administered cisplatin (20 mg/kg, i.p.). Kidney tissue was collected on day 3 after cisplatin injection. (H) The Kaplan–Meier curve for the overall survival. C57BL/6 mice were pretreated with miR-709 antagomir or anti-control (anti–miR-709, 20 mg/kg, i.p.) for 24 hours, and then administered cisplatin treatment (20 mg/kg, i.p.) for 14 days. Values are presented as mean±SEM; n= 7–14 animals per group. For each experiment, differences between means were considered statistically significant when $P<0.05$.

Recently, RG-012 has received orphan drug status from the US Food and Drug Administration and European Commission, and a phase 1 clinical study has been conducted.[46] Taken together, the success in developing medications targeting miRNA and our findings in this study indicate that anti–miR-709 could be a promising approach for developing novel therapeutics to treat AKI.

The limitation of our study is that the roles and the related mechanisms of miR-709 in mediating cisplatin-induced acute renal tubular injury were observed in mouse model and in cultured tubular cells but not in humans, as we generally do not perform biopsies on these patients. Although we did detect an upregulation of miR-709 and its correlation with the degree of kidney tissue injury in patients with AKI with ischemic or other nephrotoxic insults, the significance of miR-709 in human AKI remains to be further explored because of the limited sample size of this patient group.

In conclusion, upregulation of renal tubular miR-709 after AKI mediates mitochondrial dysfunction and cell apoptosis by depressing TFAM expression. Targeting miR-709 may serve as a new approach to preserving mitochondrial function and preventing cell death in AKI.

CONCISE METHODS

Establishment of Cisplatin-Induced AKI in Mice and Administration of miR-709 Antagomir (Anti–miR-709 Oligonucleotides)

C57BL/6 mice (male, aged 8–10 weeks old) received a single dose of cisplatin (20 mg/kg body wt) as described previously.[47,48] The control animals were injected with normal saline. Mice were euthanized 72 hours after cisplatin (479306; Sigma-Aldrich, St. Louis, MO) administration. Blood was transferred into heparinized tubes and centrifuged at 10,000×g for 10 minutes to separate the plasma, which was collected and stored at −80°C for further analysis. The kidneys collected for histology were cut along the frontal plane and fixed in 10% neutral buffered formalin overnight before being transferred to 70% ethanol. After processing and embedding the tissue in paraffin, 2–3 μm sections were prepared. The remaining kidney tissue was

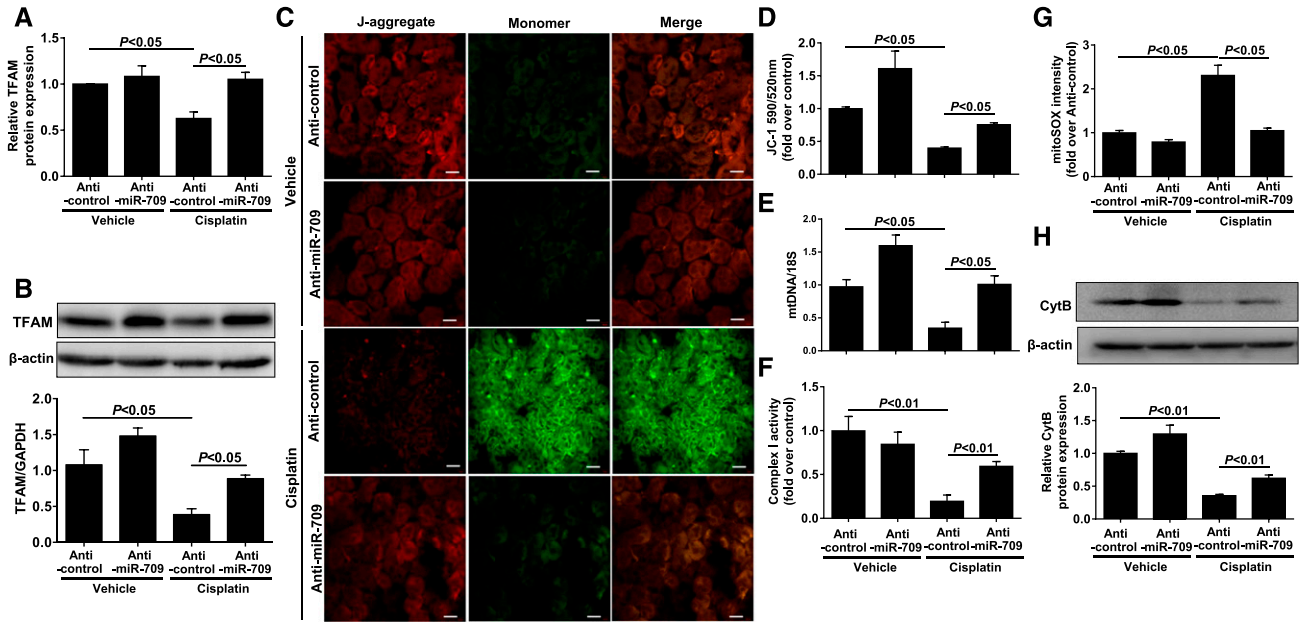

Figure 7. miR-709 antagomir attenuates kidney mitochondrial dysfunction in mouse cisplatin-induced AKI. (A) Quantitative real-time PCR (qPCR) analysis of TFAM mRNA expression. (B) Western blotting analysis of TFAM protein expression. (C) Representative confocal microscopy images of JC-1 staining; red fluorescence represents the mitochondrial aggregate JC-1 and green fluorescence indicates the monomer JC-1. Scale bar, 20 μm. (D) Quantification of JC-1 fluorescence using a FLUOstar Optima reader. (E) qPCR analysis of mtDNA copy number. (F) Complex I activity in isolated mitochondria from the kidney. (G) Quantification of the mitoSOX signal using flow cytometry. (H) Western blotting analysis of CytB protein expression. Upper panel: representative immunoblots. Lower panel: densitometric analysis. C57BL/6 mice were treated with miR-709 antagomir (anti–miR-709, 20 mg/kg, intraperitoneal) or anti-control for 24 hours and then were administered cisplatin (20 mg/kg, intraperitoneal). Kidney tissue was collected on day 3 after cisplatin injection. Data are presented as mean±SEM; n= 7 animals per group. For each experiment, differences between means were considered statistically significant when $P<0.05$.

stored at −80°C for mRNA and protein analysis. All animal experiments were performed according to a protocol approved by the Institutional Animal Care and Use Committee of Nanjing Medical University.

Oligonucleotides targeting miR-709 (miR-709 antagomir) were provided by GenePharma (Shanghai, China). The miR-709 antagomir is a 19-bp oligonucleotide conjugated to cholesterol at the 5′ terminal. The control antagomir has a comparable chemical composition, but is directed against an miRNA expressing *Caenorhabditis elegans*. For delivery of cholesterol-conjugated RNA, mice were injected intraperitoneally with an antagomir targeting miR-709 or control antagomir, at a dosage of 20 mg/kg for 24 hours before cisplatin administration.

Patients

Twenty-one patients from Peking University First Hospital with AKI and acute tubular necrosis verified by renal biopsy were enrolled in the study. Clinical parameters, including age, sex, cause of AKI, and serum creatinine levels at peak and at the time of renal biopsy were collected. AKI was diagnosed using the Kidney Disease: Improving Global Outcomes criteria.[49] Standard processing of kidney biopsy specimens included light microscopy, immunofluorescence, and electron microscopy. For light microscopy, all samples were stained with hematoxylin and eosin, periodic acid–Schiff (PAS), Masson trichrome, and Jones methenamine silver. Semiquantitative scores for tubular brush border loss and necrosis were developed by referring to the Banff Working Classification criteria.[50,51] A 0–4+ scale was applied as follows: 0= no lesion, 1+=<25%, 2+= 25% to <50%, 3+= 50% to <75%, and 4+=≥75% of parenchyma affected by the lesion. The tubular injury index (TII) was the sum of the scores for tubular brush border loss and for necrosis. The degree of tubular injury was classified as mild (TII=<2), moderate (TII=2–4), or severe (TII=≥5). Para-carcinoma kidney tissue of seven patients who underwent renal carcinoma resection, with no evidence of kidney injury through routine pathologic examination, were used as controls for the miR-709 assay. The protocol concerning the use patient samples in this study was approved by the Committee on Research Ethics of Peking University First Hospital and the Human Subjects Committee of Nanjing Medical University. Informed consent was obtained from all participants.

Fluorescence *In Situ* Hybridization

In situ hybridization was performed with probes for human or mouse miR-709 and control sequences as previously described.[52] In brief, thin sections (3 μm) of paraffin-embedded specimens from human biopsied kidney tissue or cisplatin-treated mice kidney tissue were deparaffinized and rehydrated. Sections were treated with trypsin and refixed in 4% paraformaldehyde. Then, slides were hybridized with a 5′-Cy3–labeled oligonucleotide probe complementary to miR-709 or a control probe, at 25°C for 1 hour away from light. Sections were washed in washing buffer I (4× SSC, 0.1% Tween-20), washing buffer II (2× SSC), and washing buffer III (1× SSC) three times each, and then were stained with 4′,6-diamidino-2-phenylindole for 5

minutes. After the sections were mounted with Entellan, they were viewed under a confocal microscope. Fluorescence quantitation of miR-709 was analyzed by Image-Pro Plus software.

Immunofluorescence

To visualize colocalization of miR-709 with kidney tubular protein marker, after staining with an miR-709 probe, kidney sections were incubated with primary mouse mAbs to aquaporin 1 (B-11) (1:100, sc-25287; Santa Cruz Biotechnology) at 4°C overnight. Goat anti-mouse IgG antibody conjugated to FITC (1:300, ZF-0311; ZSGB-BIO, Beijing, China) was used as a secondary antibody. Finally, sections were mounted with Clear-Mount containing 4′,6-diamidino-2-phenylindole, and visualized on a Zeiss LSM5 PASCAL confocal microscope.

Serum Creatinine, BUN, and Histology

Serum creatinine concentrations of patients and mice were analyzed in the central laboratory of our hospital using a Beckman Creatinine Analyzer II (DXC800; Beckman Coulter), which has been qualified by the National Committee for Clinical Laboratory of China. BUN was measured with a BUN Colorimetric Detection Kit (EIABUN; Invitrogen, Carlsbad, CA) according to the manufacturers' instructions. Sections at a thickness of 2 μm were used for PAS staining to evaluate histologic damage. The severity of morphologic damage was assessed in a blinded manner using an arbitrary score on the basis of PAS-stained kidney sections, following a modified protocol developed by Paller *et al.*[53] Briefly, the kidney pathology score was used for evaluating the severity of the renal injury. For each kidney, 100 cortical tubules from at least ten different views were analyzed. Higher scores represented more severe damage (maximum score per tubule was ten), with points given for the following: the presence and extent of tubular epithelial cell flattening (one point), brush border loss (one point), cell membrane bleb formation (one or two points), cytoplasmic vacuolization (one point), cell necrosis (one or two points), interstitial edema (one point), and tubular lumen obstruction (one or two points).

Cell Culture and Treatment

mPTCs, an immortalized cell line purchased from ATCC, were grown in serum-free keratinocyte medium supplemented with bovine pituitary extract and EGF (Wisent, Quebec, Canada). The cells were specifically grown at 37°C with 5% carbon dioxide and subcultured at 50%–80% confluence using 0.25% trypsin/0.02% EDTA (Invitrogen). Cisplatin was added to the serum-free medium to stimulate mPTCs. miR-709 mimic (40 nM), negative control (40 nM), miR-709 inhibitor (80 nM), and inhibitor negative control (80 nM) (GenePharma) were transfected into mPTC cells using siRNA-Mate (GenePharma) according to the manufacturer's protocol. The TFAM plasmid (pcDNA3.1-TFAM) (Addgene, Cambridge, MA) was transfected into mPTC cells using Lipofectamine 2000 (1803712; Invitrogen) according to the manufacturer's instructions.

RNA Isolation and Real-Time Quantitative PCR

Kidney cortex and cell total RNA was extracted using TRIzol (Invitrogen, Carlsbad, CA) following the manufacturer's instructions. Oligonucleotides (Table 2) were designed using Primer 5 software (available at http://frodo.wi.mit.edu/) and synthesized by Invitrogen. Real-time quantitative PCR was performed for the detection of TFAM gene expression using an ABI PRISM 7500 Sequence Detection System with SYBR Green PCR Master Mix (Roche, Mannheim, Germany). Cycling conditions were 95°C for 10 minutes, followed by 40 repeats of 95°C for 15 seconds and 60°C for 1 minute. The relative amount of mRNA was normalized to GAPDH and calculated using the $\Delta\Delta$ method from threshold cycle numbers. To detect the miRNA expression level, 250 ng of total RNA was reverse-transcribed into cDNA using an miRNA Reverse Transcription kit (Applied Biosystems, Foster City, CA). Real-time quantitative PCR was performed using a TaqMan miRNA assay kit (Applied Biosystems), which included sequence-specific primers for cDNA synthesis and TaqMan probes for real-time PCR. The relative expression was evaluated using the comparative threshold cycle method and normalized to the expression of U6 spliceosomal RNA.

Western Blotting

The kidney cortex and cells were lysed in protein lysis buffer (50 mmol/L Tris, 150 mmol/L sodium chloride, 10 mmol/L EDTA, 1% Triton X-100, 200 mmol/L sodium fluoride, 4 mmol/L sodium orthovanadate as protease inhibitors; pH 7.5) for 15 minutes on ice. The protein concentration was measured using the Bradford method. Immunoblotting was performed as previously described.[54] The primary antibodies used were as follows: primary rabbit polyclonal antibodies against TFAM (ab131607; Abcam, Cambridge, MA), CytB (sc-11436; Santa Cruz Biotechnology), and β-actin (4970; Cell Signaling Technology, Beverly, MA). Peroxidase-conjugated goat anti-rabbit secondary antibodies were purchased from Santa Cruz Biotechnology (sc-2004). Quantification was performed by measuring the intensity of the signals with the aid of the National Institutes of Health ImageJ software package.

Isolation of Mitochondria and Determination of Mitochondrial Function

Mitochondria from kidney cortex and the cultured mPTCs were isolated using a Mitochondria Isolation Kit for Tissue (89874; Thermo Fisher Scientific) according to the manufacturer's protocol. Isolated mitochondria protein concentration was determined by the Bradford method. Mitochondrial function was determined through an analysis of mtDNA copy number, $\Delta\psi$m, and mitochondrial ROS content, mitochondrial complex I activity, and OCR.

mtDNA Copy Number

Kidney cortex and cell total DNA was extracted using a DNeasy Tissue Kit (69506; QIAGEN Sciences, Germantown, MD) following the manufacturer's instructions. The primer oligonucleotides listed in Table 2 were designed using Primer 5 software and synthesized by Invitrogen. Quantitative PCR was performed for the detection of mtDNA copy number. Relative mtDNA copy numbers were normalized to the nuclear 18S rRNA gene and calculated using the $\Delta\Delta$ method from threshold cycle numbers.

$\Delta\psi m$

The $\Delta\psi$m of mPTCs and kidney tissue were monitored using JC-1, a $\Delta\psi$m-sensitive, fluorescent dye, as described previously.[55] Briefly, the

Table 2. Sequence of primer pairs for real-time quantitative PCR

Name	Forward Primer	Reverse Primer
GAPDH	5′-GTCTTCACTACCATGGAGAAGG-3′	5′-TCATGGATGACCTTGGCCAG-3′
TFAM	5′-GTCGCATCCCCTCGTCTATC-3′	5′-CCTCCTTCTCCATACCCATC-3′
mtDNA	5′-ATCCTCCCAGGATTTGGAAT-3′	5′-ACCGGTAGGAATTGCGATAA-3′
18S rRNA	5′-TTCGGAACTGAGGCCATGATT-3′	5′-TTTCGCTCTGGTCCGTCTTG-3′

frozen sections (8 μm) and adherent mPTCs were washed twice with HBSS (Sigma) and incubated in the dark with JC-1 (7.5 μM; 30 minutes at 37°C). Sections and cells were washed with JC-1 wash buffer. Fluorescence images were captured by confocal microscopy. Fluorescence quantitation was detected with flow cytometry for mPTCs and Image-Pro Plus software for frozen sections. The relative $\Delta\psi$m was calculated using the ratio of J-aggregate/monomer (590/520 nm). In healthy cells with a high $\Delta\psi$m, JC-1 enters the mitochondrial matrix in a potential dependent manner and forms aggregates. Values are expressed as the fold increase in J-aggregate/monomer fluorescence over control.

Mitochondrial ROS

Mitochondrial ROS production in mPTCs was measured using mitoSOX (M36008; Invitrogen) as described previously.[55] For quantitation of mitochondrial ROS production, the ROS levels were analyzed by flow cytometry. For measurement of kidney tissue mitochondrial ROS levels, 50 μg of isolated mitochondrial protein was stained with mitoSOX and incubated for 10 minutes. The fluorescence intensity was analyzed on a FLUOstar Optima reader at excitation/emission wave lengths of 490/530 nm. Data are expressed as fluorescence units per milligram of protein.

Mitochondrial Complex I Activity

Mitochondrial OXPHOS complex I (NADH dehydrogenase) enzyme activity was measured by a Complex I Enzyme Activity Microplate Assay Kit (Colorimetric) (ab109721; Abcam) according to the manufacturers' protocols. Briefly, isolated mitochondria samples were prepared at final protein concentration of 5.5 mg/ml, and the samples were loaded to the wells of the microplate. The microplate was incubated for 3 hours at room temperature. Then 200 μl of assay solution was added to each well. Optical density (OD 450 nm) was measured in a kinetic mode at room temperature for 30 minutes.

OCR

An assay using the Seahorse XF-96 Extracellular Flux Analyzer (Seahorse Bioscience, Copenhagen, Denmark) was performed to measure the OCR. Briefly, mPTCs were initially transfected with negative control, miR-709 mimics, or TFAM plasmid for 24 hours before cisplatin treatment. On the time of the experiment, cell media was replaced by Seahorse assay media and cells were incubated at 37°C in a carbon dioxide-free incubator for 1 hour before assessing basal OCR. Inhibitors were prepared in the same medium and the injection ports of the sensors were filled. Thirty minutes before the experiment, the sensor was placed into the XF-96 instrument and calibration was initiated. After calibration, the basal oxygen consumption was recorded for 20 minutes and OCR measurements were performed over time upon the successive addition of the mitochondrial inhibitors: oligomycin (1 μM), which blocks the proton channel of the portion of ATP synthase (complex V) and thus inhibits ATP synthesis is used to determine ATP-synthesis coupling efficiency; the uncoupler carbonyl cyanide 4-trifluoromethoxy-phenylhydrazone (0.5 μM) was used to calculate the spare respiratory capacity; and finally, a mixture of rotenone (0.5 μM) and antimycin A (0.5 μM), inhibiting complex I and complex III respectively, was used to assess the consumption of oxygen of nonmitochondrial origin.

Plasmid Construction and Luciferase Reporter Assay

The 3′-UTR of TFAM was obtained *via* PCR using human genomic DNA, and inserted downstream of the pGL3 promoter (Promega, Madison, WI). Site-directed mutagenesis was conducted to create mutations in the region corresponding to the miR-709 seed sequence. For the luciferase reporter assay, the resulting constructs were co-transfected with Renilla luciferase into mPTCs using Lipofectamine 2000. At 24 hours after transfection, cells were assayed using a Dual-Luciferase Report Assay System (Promega). The firefly luciferase activity was normalized to the corresponding Renilla luciferase activity.

Apoptosis Analysis

Apoptosis was tested with terminal deoxynucleotidyl transferase–mediated digoxigenin-deoxyuridine nick-end labeling (TUNEL) *in situ* hybridization in human and mouse kidney sections, and through annexin-V–FITC and propidium iodide (PI) staining and a caspase-3 activity assay in cultured mPTCs.

TUNEL Assay

An *in situ* cell death detection kit was used according to the manufacturer's instructions for TUNEL assays (Roche). TUNEL-positive tubular cells were counted in ten nonoverlapping fields of each sample.

Annexin-V–FITC and PI Staining

After treatment, the cells were double-stained with annexin-V–FITC and PI (Annexin-V–FITC Apoptosis Detection Kit; BD Biosciences, San Diego, CA) according to the manufacturer's instructions. Quantification was then performed using flow cytometry.

Caspase-3 Activity Assay

Caspase-3 activity in mPTCs was measured using a caspase activity assay kit (Beyotime, Hangzhou, China) through cleavage of a colorless substrate specific for caspase-3 (Ac-DEVD-pNA) and release of the chromophore *p*-nitroaniline. The absorbance of *p*-nitroaniline was determined at 405 nm.

Cell Counting Kit 8 Assay

Cell proliferation was determined by the Cell Counting Kit 8 assay kit (C0037; Beyotime). Briefly, 10 μl Cell Counting Kit 8 reagent was added to mPTCs transfected with TFAM small interfering RNA for 48 hours and incubated for 2 hours. The absorbance was detected at 450 nm.

Statistical Analyses

All data are presented as mean±SEM or median and 25th–75th percentile. Statistical analysis was performed with one-way ANOVA followed by Bonferroni test or unpaired *t* test, using SPSS v19 statistical software (SPSS Inc., Chicago, IL). Associations between groups were determined by Spearman rank correlation. Comparison of survival curves was determined by log-rank (Mantel–Cox) test. $P<0.05$ was considered significant.

ACKNOWLEDGMENTS

This work was supported by grants from the National Natural Science Foundation of China (81625004, 81325004, 81530023, 81370802, 81300591, and 81270797), the National Key Research and Development Program (2016YFC0906103), and the Natural Science Foundation of Jiangsu Province (BK20141079, and BL2014007).

DISCLOSURES

None.

REFERENCES

1. Kohli HS, Bhat A, Jairam A, Aravindan AN, Sud K, Jha V, Gupta KL, Sakhuja V: Predictors of mortality in acute renal failure in a developing country: A prospective study. *Ren Fail* 29: 463–469, 2007
2. Rewa O, Bagshaw SM: Acute kidney injury-epidemiology, outcomes and economics. *Nat Rev Nephrol* 10: 193–207, 2014
3. Morigi M, Rota C, Remuzzi G: Mesenchymal stem cells in kidney repair. *Methods Mol Biol* 1416: 89–107, 2016
4. Sawhney S, Mitchell M, Marks A, Fluck N, Black C: Long-term prognosis after acute kidney injury (AKI): What is the role of baseline kidney function and recovery? A systematic review. *BMJ Open* 5: e006497, 2015
5. KDIGO. Clinical Practice Guideline for Acute Kidney Injury: Prevention and treatment of AKI. *Kidney Int Suppl (2011)* 2: 37–68, 2012
6. Duann P, Lianos EA, Ma J, Lin PH: Autophagy, innate immunity and tissue repair in acute kidney injury. *Int J Mol Sci* 17: 662, 2016
7. Marullo R, Werner E, Degtyareva N, Moore B, Altavilla G, Ramalingam SS, Doetsch PW: Cisplatin induces a mitochondrial-ROS response that contributes to cytotoxicity depending on mitochondrial redox status and bioenergetic functions. *PLoS One* 8: e81162, 2013
8. Yang Y, Liu H, Liu F, Dong Z: Mitochondrial dysregulation and protection in cisplatin nephrotoxicity. *Arch Toxicol* 88: 1249–1256, 2014
9. Nowak G: Protein kinase C-alpha and ERK1/2 mediate mitochondrial dysfunction, decreases in active Na+ transport, and cisplatin-induced apoptosis in renal cells. *J Biol Chem* 277: 43377–43388, 2002
10. Park MS, De Leon M, Devarajan P: Cisplatin induces apoptosis in LLC-PK1 cells via activation of mitochondrial pathways. *J Am Soc Nephrol* 13: 858–865, 2002
11. Leelahavanichkul A, Somparn P, Panich T, Chancharoenthana W, Wongphom J, Pisitkun T, Hirankarn N, Eiam-Ong S: Serum miRNA-122 in acute liver injury induced by kidney injury and sepsis in CD-1 mouse models. *Hepatol Res* 45: 1341–1352, 2015
12. Ambros V: The functions of animal microRNAs. *Nature* 431: 350–355, 2004
13. Chang S, Johnston RJ Jr., Frøkjaer-Jensen C, Lockery S, Hobert O: MicroRNAs act sequentially and asymmetrically to control chemosensory laterality in the nematode. *Nature* 430: 785–789, 2004
14. Gregory RI, Chendrimada TP, Cooch N, Shiekhattar R: Human RISC couples microRNA biogenesis and posttranscriptional gene silencing. *Cell* 123: 631–640, 2005
15. Winter J, Jung S, Keller S, Gregory RI, Diederichs S: Many roads to maturity: MicroRNA biogenesis pathways and their regulation. *Nat Cell Biol* 11: 228–234, 2009
16. Prajapati P, Sripada L, Singh K, Bhatelia K, Singh R, Singh R: TNF-α regulates miRNA targeting mitochondrial complex-I and induces cell death in dopaminergic cells. *Biochim Biophys Acta* 1852: 451–461, 2015
17. Fan S, Chen WX, Lv XB, Tang QL, Sun LJ, Liu BD, Zhong JL, Lin ZY, Wang YY, Li QX, Yu X, Zhang HQ, Li YL, Wen B, Zhang Z, Chen WL, Li JS: miR-483-5p determines mitochondrial fission and cisplatin sensitivity in tongue squamous cell carcinoma by targeting FIS1. *Cancer Lett* 362: 183–191, 2015
18. Mao C, Zhang J, Lin S, Jing L, Xiang J, Wang M, Wang B, Xu P, Liu W, Song X, Lv C: MiRNA-30a inhibits AECs-II apoptosis by blocking mitochondrial fission dependent on Drp-1. *J Cell Mol Med* 18: 2404–2416, 2014
19. Bai XY, Ma Y, Ding R, Fu B, Shi S, Chen XM: miR-335 and miR-34a promote renal senescence by suppressing mitochondrial antioxidative enzymes. *J Am Soc Nephrol* 22: 1252–1261, 2011
20. Jiang L, Qiu W, Zhou Y, Wen P, Fang L, Cao H, Zen K, He W, Zhang C, Dai C, Yang J: A microRNA-30e/mitochondrial uncoupling protein 2 axis mediates TGF-β1-induced tubular epithelial cell extracellular matrix production and kidney fibrosis. *Kidney Int* 84: 285–296, 2013
21. Chen H, Mo D, Li M, Zhang Y, Chen L, Zhang X, Li M, Zhou X, Chen Y: miR-709 inhibits 3T3-L1 cell differentiation by targeting GSK3β of Wnt/β-catenin signaling. *Cell Signal* 26: 2583–2589, 2014
22. Liu T, Zhang X, Sha K, Liu X, Zhang L, Wang B: miR-709 up-regulated in hepatocellular carcinoma, promotes proliferation and invasion by targeting GPC5. *Cell Prolif* 48: 330–337, 2015
23. Li M, Chen H, Chen L, Chen Y, Liu X, Mo D: miR-709 modulates LPS-induced inflammatory response through targeting GSK-3β. *Int Immunopharmacol* 36: 333–338, 2016
24. Ikeda M, Ide T, Fujino T, Arai S, Saku K, Kakino T, Tyynismaa H, Yamasaki T, Yamada K, Kang D, Suomalainen A, Sunagawa K: Overexpression of TFAM or twinkle increases mtDNA copy number and facilitates cardioprotection associated with limited mitochondrial oxidative stress. *PLoS One* 10: e0119687, 2015
25. Szeto HH, Liu S, Soong Y, Seshan SV, Cohen-Gould L, Manichev V, Feldman LC, Gustafsson T: Mitochondria protection after acute ischemia prevents prolonged upregulation of IL-1β and IL-18 and arrests CKD. *J Am Soc Nephrol* 28: 1437–1449, 2017
26. Lan R, Geng H, Singha PK, Saikumar P, Bottinger EP, Weinberg JM, Venkatachalam MA: Mitochondrial pathology and glycolytic shift during proximal tubule atrophy after ischemic AKI. *J Am Soc Nephrol* 27: 3356–3367, 2016
27. Peres LA, da Cunha AD Jr.: Acute nephrotoxicity of cisplatin: Molecular mechanisms. *J Bras Nefrol* 35: 332–340, 2013
28. Tábara LC, Poveda J, Martin-Cleary C, Selgas R, Ortiz A, Sanchez-Niño MD: Mitochondria-targeted therapies for acute kidney injury. *Expert Rev Mol Med* 16: e13, 2014
29. Unuma K, Aki T, Funakoshi T, Yoshida K, Uemura K: Cobalt protoporphyrin accelerates TFEB activation and lysosome reformation during LPS-induced septic insults in the rat heart. *PLoS One* 8: e56526, 2013
30. Tsuji N, Tsuji T, Ohashi N, Kato A, Fujigaki Y, Yasuda H: Role of mitochondrial DNA in septic AKI via toll-like receptor 9. *J Am Soc Nephrol* 27: 2009–2020, 2016
31. Parikh SM, Yang Y, He L, Tang C, Zhan M, Dong Z: Mitochondrial function and disturbances in the septic kidney. *Semin Nephrol* 35: 108–119, 2015
32. Xia N, Yan RY, Liu Q, Liao XH, Sun H, Guo H, Zhang L: Augmenter of liver regeneration plays a protective role against hydrogen

peroxide-induced oxidative stress in renal proximal tubule cells. *Apoptosis* 20: 423–432, 2015
33. Parikh SM: Therapeutic targeting of the mitochondrial dysfunction in septic acute kidney injury. *Curr Opin Crit Care* 19: 554–559, 2013
34. Jacobs ME, Jeffers LA, Welch AK, Wingo CS, Cain BD: MicroRNA regulation of endothelin-1 mRNA in renal collecting duct cells. *Life Sci* 118: 195–199, 2014
35. Tamminga J, Kathiria P, Koturbash I, Kovalchuk O: DNA damage-induced upregulation of miR-709 in the germline downregulates BORIS to counteract aberrant DNA hypomethylation. *Cell Cycle* 7: 3731–3736, 2008
36. Tang X, Gal J, Zhuang X, Wang W, Zhu H, Tang G: A simple array platform for microRNA analysis and its application in mouse tissues. *RNA* 13: 1803–1822, 2007
37. Maes OC, An J, Sarojini H, Wang E: Murine microRNAs implicated in liver functions and aging process. *Mech Ageing Dev* 129: 534–541, 2008
38. Surendran S, Jideonwo VN, Merchun C, Ahn M, Murray J, Ryan J, Dunn KW, Kota J, Morral N: Gene targets of mouse miR-709: Regulation of distinct pools. *Sci Rep* 6: 18958, 2016
39. Kukat C, Davies KM, Wurm CA, Spåhr H, Bonekamp NA, Kühl I, Joos F, Polosa PL, Park CB, Posse V, Falkenberg M, Jakobs S, Kühlbrandt W, Larsson NG: Cross-strand binding of TFAM to a single mtDNA molecule forms the mitochondrial nucleoid. *Proc Natl Acad Sci U S A* 112: 11288–11293, 2015
40. Larsson NG, Wang J, Wilhelmsson H, Oldfors A, Rustin P, Lewandoski M, Barsh GS, Clayton DA: Mitochondrial transcription factor A is necessary for mtDNA maintenance and embryogenesis in mice. *Nat Genet* 18: 231–236, 1998
41. Uchiumi T, Kang D: The role of TFAM-associated proteins in mitochondrial RNA metabolism. *Biochim Biophys Acta* 1820: 565–570, 2012
42. Kanki T, Ohgaki K, Gaspari M, Gustafsson CM, Fukuoh A, Sasaki N, Hamasaki N, Kang D: Architectural role of mitochondrial transcription factor A in maintenance of human mitochondrial DNA. *Mol Cell Biol* 24: 9823–9834, 2004
43. Stiles AR, Simon MT, Stover A, Eftekharian S, Khanlou N, Wang HL, Magaki S, Lee H, Partynski K, Dorrani N, Chang R, Martinez-Agosto JA, Abdenur JE: Mutations in TFAM, encoding mitochondrial transcription factor A, cause neonatal liver failure associated with mtDNA depletion. *Mol Genet Metab* 119: 91–99, 2016
44. Hall AM, Schuh CD: Mitochondria as therapeutic targets in acute kidney injury. *Curr Opin Nephrol Hypertens* 25: 355–362, 2016
45. Gomez IG, MacKenna DA, Johnson BG, Kaimal V, Roach AM, Ren S, Nakagawa N, Xin C, Newitt R, Pandya S, Xia TH, Liu X, Borza DB, Grafals M, Shankland SJ, Himmelfarb J, Portilla D, Liu S, Chau BN, Duffield JS: Anti-microRNA-21 oligonucleotides prevent Alport nephropathy progression by stimulating metabolic pathways. *J Clin Invest* 125: 141–156, 2015
46. Regulus: Study of weekly RG-012 injections in patients with alport syndrome (HERA). Available at: http://regulusrx.com/programs/pipeline/rg-012/. Accessed July 28, 2016
47. Zhu HY, Liu MY, Hong Q, Zhang D, Geng WJ, Xie YS, Chen XM: Role of microRNA-181a in the apoptosis of tubular epithelial cell induced by cisplatin. *Chin Med J (Engl)* 125: 523–526, 2012
48. Wei Q, Dong G, Yang T, Megyesi J, Price PM, Dong Z: Activation and involvement of p53 in cisplatin-induced nephrotoxicity. *Am J Physiol Renal Physiol* 293: F1282–F1291, 2007
49. Matzke GR, Aronoff GR, Atkinson AJ Jr., Bennett WM, Decker BS, Eckardt KU, Golper T, Grabe DW, Kasiske B, Keller F, Kielstein JT, Mehta R, Mueller BA, Pasko DA, Schaefer F, Sica DA, Inker LA, Umans JG, Murray P: Drug dosing consideration in patients with acute and chronic kidney disease-a clinical update from Kidney Disease: Improving Global Outcomes (KDIGO). *Kidney Int* 80: 1122–1137, 2011
50. Solez K, Colvin RB, Racusen LC, Haas M, Sis B, Mengel M, Halloran PF, Baldwin W, Banfi G, Collins AB, Cosio F, David DS, Drachenberg C, Einecke G, Fogo AB, Gibson IW, Glotz D, Iskandar SS, Kraus E, Lerut E, Mannon RB, Mihatsch M, Nankivell BJ, Nickeleit V, Papadimitriou JC, Randhawa P, Regele H, Renaudin K, Roberts I, Seron D, Smith RN, Valente M: Banff 07 classification of renal allograft pathology: Updates and future directions. *Am J Transplant* 8: 753–760, 2008
51. Racusen LC, Solez K, Colvin RB, Bonsib SM, Castro MC, Cavallo T, Croker BP, Demetris AJ, Drachenberg CB, Fogo AB, Furness P, Gaber LW, Gibson IW, Glotz D, Goldberg JC, Grande J, Halloran PF, Hansen HE, Hartley B, Hayry PJ, Hill CM, Hoffman EO, Hunsicker LG, Lindblad AS, Marcussen N, Mihatsch MJ, Nadasdy T, Nickerson P, Olsen TS, Papadimitriou JC, Randhawa PS, Rayner DC, Roberts I, Rose S, Rush D, Salinas-Madrigal L, Salomon DR, Sund S, Taskinen E, Trpkov K, Yamaguchi Y: The Banff 97 working classification of renal allograft pathology. *Kidney Int* 55: 713–723, 1999
52. Jiang L, Lin C, Song L, Wu J, Chen B, Ying Z, Fang L, Yan X, He M, Li J, Li M: MicroRNA-30e* promotes human glioma cell invasiveness in an orthotopic xenotransplantation model by disrupting the NF-κB/IκBα negative feedback loop. *J Clin Invest* 122: 33–47, 2012
53. Paller MS, Hoidal JR, Ferris TF: Oxygen free radicals in ischemic acute renal failure in the rat. *J Clin Invest* 74: 1156–1164, 1984
54. Zhang A, Jia Z, Guo X, Yang T: Aldosterone induces epithelial-mesenchymal transition via ROS of mitochondrial origin. *Am J Physiol Renal Physiol* 293: F723–F731, 2007
55. Yuan Y, Huang S, Wang W, Wang Y, Zhang P, Zhu C, Ding G, Liu B, Yang T, Zhang A: Activation of peroxisome proliferator-activated receptor-γ coactivator 1α ameliorates mitochondrial dysfunction and protects podocytes from aldosterone-induced injury. *Kidney Int* 82: 771–789, 2012